CD39^{+}PD-1^{+}CD8^{+} T cells mediate metastatic dormancy in breast cancer

Paulino Tallón de Lara[1,2,5,*], Héctor Castañón Cuadrado[1,2,*], Marijne Vermeer[1,2,**], Nicolás Núñez[1,2,**], Karina Silina[1,2], Bettina Sobottka[3], Joaquín Urdínez[4], Virginia Cecconi[1,2], Farkhondeh Movahedian Attar[1,2], Stefanie Hiltbrunner[1,2,6] Isabelle Glarner[1,2], Holger Moch[3], Sònia Tugues[1,2], Burkhard Becher[1,2], Maries van den Broek[1,2,7]

[1]Institute of Experimental Immunology, University of Zurich, Zurich, Switzerland. [2]Comprehensive Cancer Center Zurich, Zurich, Switzerland. [3]Department of Pathology and Molecular Pathology, University Hospital Zurich, Switzerland. [4]Department of Orthopaedics, Balgrist University Hospital, University of Zurich Zurich, Switzerland. [5]Current address: Department of Medicine, Mount Sinai St. Luke's & Mount Sinai West, Icahn School of Medicine at Mount Sinai, New York, NY, USA. [6]Current address: Department of Hematology and Oncology, University Hospital Zurich, Zurich, Switzerland. [7]Corresponding author. Maries van den Broek, Institute of Experimental Immunology, University of Zurich, Winterthurerstrasse 190, 8057 Zurich, Switzerland. E-mail: vandenbroek@immunology.uzh.ch.

[*]Equal first-author contribution. [**]Equal second-author contribution.

Summary

Some breast tumors metastasize aggressively whereas others remain in a state of metastatic dormancy for months or even years. The mechanism governing such metastatic dormancy remains largely unknown. Through high-parametric single-cell mapping, we identified a discrete population of $CD39^+PD\text{-}1^+CD8^+$ T cells present both in primary tumors and in dormant metastasis, which was hardly found in aggressively metastasizing tumors. Of note, the adoptive transfer of purified $CD39^+PD\text{-}1^+CD8^+$ T cells prevented metastatic outgrowth. In human breast cancer, the frequency of $CD39^+PD\text{-}1^+CD8^+$ but not of total $CD8^+$ T cells correlated with delayed metastatic relapse after resection (disease-free survival), thus underlining the biological relevance of $CD39^+PD\text{-}1^+CD8^+$ T cells for controlling experimental and human breast cancer. Furthermore, density of $CD39^+PD\text{-}1^+CD8^+$ T cells may serve as a novel biomarker and may serve as a potential immunotherapy target. Here, we discovered that a primary breast tumor primes a systemic, $CD39^+PD\text{-}1^+CD8^+$ T cell response that is essential for metastatic dormancy in the lungs.

Introduction

Metastasis is the major cause of death in patients with breast cancer. The metastatic behavior of this disease is heterogeneous regarding affected organs as well as timing[1,2]. Whereas some patients develop metastasis shortly after or even before diagnosis, others show metastatic lesions only years or decades after removal of the primary tumor[1,3]. In fact, approximately 20% of disease-free patients will relapse within 7 years after resection, and patients that appear to be cured from breast cancer have a higher mortality than the rest of the population even 20 years after surgery[4,5]. Such late relapses are thought to result from disseminated cancer cells (DCCs) that reached different organs but remained dormant for several years[6]. Indeed, the presence of DCCs in the bone marrow of breast cancer patients loosely correlates with the development of metastatic relapse[7,8].

The cancer cell-intrinsic and -extrinsic mechanisms governing metastatic dormancy are poorly understood. Some cancer cell-intrinsic factors have been associated with dormancy such as inhibition of the PI3K-AKT pathway[9], activation of p38 or triggering of an endoplasmic reticulum stress response[10]. In addition, the microenvironment in the (pre)metastatic organ may induce dormancy[11] by different signals such as an endothelial cell-derived thrombospondin-1[12] or TGF-β2 produced in the bone marrow[13]. Only few studies addressed the influence of cancer cell-extrinsic factors such as innate[14,15] and adaptive immunity[16,17] on dormancy. Although infiltration of the primary tumor by T cells was shown to correlate with a good prognosis[18], it

remains unclear whether this correlation is explained by cytotoxic T cells that eliminate cancer cells or by T cells that prevent the outgrowth of cancer cells and induce dormancy[19,20].

Here we sought to understand the mechanism that governs metastatic dormancy of DCCs and discovered that the primary tumor primes a systemic, $CD8^+$ T cell response that prevents metastatic outgrowth of DCCs in the lungs. The protective T cells expressed markers that are generally associated with activation and exhaustion. Promoting such a response may provide a rationale for development of future immunotherapies that aim to prevent metastatic relapse.

Results

Disseminated 4T07 breast cancer cells are dormant

We used two preclinical models for breast cancer that were originally derived from the same spontaneous tumor in BALB/c mice, 4T1 and 4T07[21] (Figure 1A). 4T1 orthotopic breast cancer produces macro-metastasis in different organs[22,23], whereas 4T07 is essentially non-metastatic. Some studies, however, showed the presence of disseminated 4T07 cells in distal organs[21,24]. Orthotopically injected 4T1 and 4T07 cells showed comparable breast cancer growth and incidence in immunocompetent BALB/c mice, although 4T1 tumors grew faster at late stages (Figures 1B and 1C). But, whereas 4T1 breast cancer readily induced aggressively growing lung metastasis, 4T07 did not (Figure 1D). Despite absence of macro-metastasis, we found disseminated 4T07 cells in the lungs (Extended Data Figure 1A) of all mice, suggesting that 4T07 DCCs seed the lungs but fail to grow out. Presence of dormant DCCs in the lungs of all mice bearing a 4T07-mCh primary tumor was confirmed by immunofluorescence (Figures 1E and Extended Data Figure 1B). Disseminated 4T07 cells were present as single cells and were Ki67-negative, as has been previously described for dormant DCCs[15,17]. The fact that we found non-proliferating, disseminated 4T07 21 days after resection of the primary tumor (Figures 1F and 1G) further underscores the dormant state of 4T07 DCCs.

Breast cancer induces $CD8^+$ T cell-mediated immunity resulting in dormancy

We first investigated whether cancer cell-intrinsic features influenced the outgrowth of DCCs in the lungs by injecting 4T1 or 4T07 breast cancer cells intravenously (i.v.) into naïve mice (Figure 2A). Under these experimental conditions, both cell lines comparably formed macro-metastases (Figure 2B), suggesting that both cell lines can progressively grow in the lungs.

The myeloid cell compartment was shown to undergo cancer-induced changes that promote metastasis by creating a pre-metastatic niche in the 4T1 model[25,26]. Specifically, 4T1 primary tumors induce systemic neutrophilia[27] and splenomegaly[26], as well as accumulation of inflammatory monocytes[28], eosinophils, neutrophils[27] and alveolar macrophages[29] in the pre-metastatic lung. We therefore compared 4T1- and 4T07-induced changes on the myeloid compartment in blood and lungs and observed no differences regarding splenomegaly (Extended Data Figure 2A), or neutrophilia (Extended Data Figure 2B). The lungs of mice with 4T1 or 4T07 breast cancer were similar concerning the presence of inflammatory monocytes (Extended Data Figure 2C), neutrophils (Extended Data Figure 2D), eosinophils (Extended Data Figure 2E) and alveolar macrophages (Extended Data Figure 2F) as determined by flow cytometry (Extended Data Figure 2G). We saw the previously reported accumulation of myeloid cells in the lungs during breast cancer progression[27] in 4T1 and 4T07 alike (Extended Data Figure 2). Thus, the difference in metastatic behavior of 4T1 and 4T07 breast cancer cannot be explained by systemic changes in the myeloid compartment.

Orthotopic 4T07 tumors induced progressively growing lung metastases in T cell-deficient BALB/c *Foxn1*$^{nu/nu}$ mice, whereas T cell-deficiency hardly

influenced metastatic behavior of 4T1 tumors (Figures 2C, 2D and 2E). To compare lung metastases in both strains, we analyzed wild type and *Foxn1*$^{nu/nu}$ mice at the same time point after injection and added an additional group of wild type mice in which breast tumors were allowed to progress until they matched the size in *Foxn1*$^{nu/nu}$ mice (WT late) (Figures 2D and 2E). Thus, metastatic dormancy of disseminated 4T07 breast cancer cells completely depends on T cells. To study whether CD8^{+} T cells are responsible for metastatic dormancy, we depleted CD8^{+} T cells from mice followed by orthotopic injection of 4T07 cells and subsequent analysis of lung metastatic load by IVIS (Figure 2F). While the growth of primary tumors was unaffected by CD8-depletion, disseminated 4T07-LZ cells grew out to macro-metastases in the absence of CD8^{+} T cells (Figures 2G and 2H), suggesting that primary 4T07 breast cancer induces CD8^{+} T cell-dependent immunity that is essential for metastatic dormancy.

To corroborate this, we orthotopically injected untagged 4T07 cells (or PBS as control) followed by an i.v. challenge with luciferase-tagged 4T07-LZ cells 11 days later (Figure 2I). If the primary tumor had induced protective immunity, we would expect a reduction of lung metastatic load. Because we measured lung metastatic load by bioluminescence, we specifically quantified the i.v. injected, luciferase-tagged 4T07 cells. The presence of a primary 4T07 tumor prevented metastatic outgrowth of i.v. injected 4T07 cells (Figures 2J and 2K) and resulted in the presence of disseminated, non-cycling single 4T07 cells in the lungs (Extended Data Figures 3A and 3B). Resection of the primary tumor before i.v. challenge did not interfere with dormancy (Extended Data Figures 3C and 3D),

whereas depletion of CD8$^+$ cells enabled metastatic outgrowth (Extended Data Figures 3E and 3F). In contrast, 4T1 breast cancer did not protect against experimental 4T1 lung metastasis (Extended Data Figures 3G and 3H). Together, these data suggest that 4T07 breast cancer induces a systemic, protective memory response that mediates dormancy of DCCs.

CD39$^+$PD-1$^+$CD8$^+$ T cells mediate metastatic dormancy

First, we analyzed the presence of different immune cells in primary 4T1 and 4T07 tumors (Extended Data Figure 4A). We found no differences in the number of eosinophils (Extended Data Figure 4B), neutrophils (Extended Data Figure 4C), NK cells (Extended Data Figure 4D) or inflammatory monocytes (Extended Data Figure 4E), but 4T1 tumors contained a higher number of macrophages than 4T07 tumors (Extended Data Figure 4F).

Since we found that 4T07 metastatic dormancy depends on CD8$^+$ T cells, we characterized these cells in 4T1 and 4T07 primary tumors by high-dimensional flow cytometry. First, we gated on T cells (Extended Data Figure 5A), visualized all the markers in our 23-parameter panel using a two-dimensional *t*-stochastic neighbor embedding (tSNE) projection[30] (Figure 3A) and clustered the cells using FlowSOM[31,32] (Figures 3A and 3B, upper panels and lower left panel). Based on the median marker intensities observed in the clusters (Figure 3B, lower right panel), we annotated the major cell populations (CD8$^+$ T cells, CD4$^+$ T cells, and CD4$^+$ CD25$^+$ regulatory T cells) and determined their frequency and the position of each population in the tSNE projection. The frequency of regulatory T cells was similar in 4T1 and 4T07 tumors, while conventional CD4$^+$

cells were more abundant in 4T1 tumors compared to 4T07. In contrast, 4T07 primary tumors contained a higher proportion of $CD8^+$ T cells (Figure 3B, lower left panel).

Of note, within the CD8 compartment (Figure 3C), we observed that 4T07 breast cancer accumulated $CD39^+PD\text{-}1^+CD8^+$ T cells (Figure 3D). To substantiate that enrichment of $CD39^+PD\text{-}1^+CD8^+$ T cells is the key immunological difference between 4T07 and 4T1 breast cancers, we analyzed our high-dimensional flow cytometry data using the representation-learning algorithm CellCnn[33,34]. In agreement with FlowSOM analysis, CellCnn detected a population with high expression of CD39, PD-1, LAG3 and Tim-3. Indeed, the two markers that best defined the population and showed the biggest differential abundance in terms of the Kolmogorov–Smirnov two-sample test between the whole-cell population and the selected cell subsets (higher KS value) were PD-1 and CD39 (Figure 3E). This population expressed more TNFα, CTLA-4, Tbet and Ki67 (Figures 3E and 3F, Extended Data Figure 5B) and was more abundant in 4T07 compared to 4T1 tumors (Figures 3G and 3H). In addition, $CD39^+PD\text{-}1^+CD8^+$ T cells expressed more of LAG-3 and Tim-3 (Figure 3F), which characterizes this population as effector cells that experienced recent T cell receptor engagement[35,36] but may also indicate exhaustion[37,38]. Importantly, this population is found in the lungs of mice with primary 4T07 breast cancer (Figure 3I). A proportion of this population expresses CD103, hence resembling tissue-resident memory T cells[39,40] (Figure 3J). Our observation that $CD39^+PD\text{-}1^+CD8^+$ T cells didn't express CD103 in the primary tumor (Figure 3F) is in line with recent data showing that

tissue-resident-like memory cells in human breast cancer are CD103-negative[41]. Thus, accumulation of CD39$^+$PD-1$^+$CD8$^+$ T cells is the main immunological difference between dormant and metastatic tumors.

To investigate whether the CD39$^+$PD-1$^+$CD8$^+$ T population can control metastasis formation and therefore mediates metastatic dormancy, we sorted those cells from 4T07 breast cancer and adoptively transferred them to naïve BALB/c mice followed by an i.v. injection of 4T07-LZ cells (Figures 4A and 4B). Adoptive transfer of CD39$^+$PD-1$^+$CD8$^+$ T cells prevented 4T07 lung metastasis, whereas injection of PBS or CD8$^+$ T cells lacking CD39$^+$PD-1$^+$ cells (referred to as other CD8$^+$ T cells) did not (Figures 4C and 4D). Thus, our results suggest that CD39$^+$PD-1$^+$CD8$^+$ T cells control disseminated 4T07 breast cancer cells.

The presence of non-proliferating disseminated 4T07 cells in the lungs suggests that CD8$^+$ T cells mediate dormancy by cell cycle arrest. Therefore, we tested whether CD39$^+$PD-1$^+$CD8$^+$ T cell-derived IFNγ and TNFα induce senescence[42] by exposing 4T07 cells to those cytokines in vitro. We observed a significant increase in the number of senescent cells as measured by expression of senescence-associated β-galactosidase activity (Extended Data Figures 6A and 6B).

Thus, 4T07 primary tumors prime systemic CD8$^+$ T cells that presumably induce cell cycle arrest of DCCs and prevent overt metastatic disease.

CD39$^+$PD-1$^+$CD8$^+$ T cells have a transcriptome rich in exhaustion and effector molecules

To understand why this population controls DCCs, we sorted CD39$^+$PD-1$^+$CD8$^+$ and other CD8$^+$ T cells from 4T07 breast cancer and compared their transcriptome (Figures 5A and 5B). CD39$^+$PD-1$^+$CD8$^+$ cells show overrepresentation of transcripts associated with effector function including *Prf1, Fasl, Gzmf, Gzme, Gzmd, Gzmc, Gzmb, Gzmk and Ifng* (Figure 5C). This was confirmed by gene set enrichment analysis (GSEA)[43] showing that the transcriptome of the sorted CD39$^+$PD-1$^+$CD8$^+$ cells shows strong similarities with human tissue-resident CD8$^+$ T cells (Figure 5D), which were recently shown to correlate with improved survival in triple negative breast cancer[19]. This is in line with their unique capacity cells to prevent metastatic progression. Furthermore, the fact that dormancy is never observed in 4T1 breast cancer is explained by the low number of such protective T cells in 4T1-bearing hosts (Figure 3) and not by their transcriptional signature, since CD39$^+$PD-1$^+$CD8$^+$ cells from 4T1 and 4T07 tumors did not show many differences (Extended Data Figure 7A). The transcriptome of CD39$^+$PD-1$^+$CD8$^+$ cells was also enriched in markers of activation and exhaustion such as *Vsir* (VISTA), *Tnfrsf18* (GITR), *Tigit*, *Cd224* (2B4), *Tnfrsf9* (4-1BB), *Tnfrsf4* (OX-40), *Icos*, *Lag-3*, *Ctla4* and *Havcr2* (Tim-3). This is consistent with their overexpression of the transcription factor TOX (Figure 5C) which leads to expression of exhaustion markers and persistence of effector function during chronic antigen stimulation[44].

Taken together, CD39$^+$PD-1$^+$CD8$^+$ cells have a unique transcriptomic signature defined by the co-expression of immune checkpoint molecules and effector proteins.

$CD39^+PD\text{-}1^+CD8^+$ but not total $CD8^+$ T cells correlate with increased disease-free after resection survival in breast cancer patients

To investigate the clinical relevance of our preclinical findings, we analyzed primary breast cancer tissues from a cohort of 54 patients, who had a metastatic relapse after primary tumor resection (Table 1) for the presence of CD8, CD39, PD-1 and epithelial cells using 5-plex immunofluorescence (Figure 6A). Our cohort shows the typical survival curves for the individual subtypes, suggesting that it is representative (Extended Data Figure 8A). Patients with a high density of intra-tumoral $CD39^+PD\text{-}1^+CD8^+$ T cells had a significantly longer disease-free survival after surgery than patients with a low density of such cells (Figure 6B). The density of extra-tumoral $CD39^+PD\text{-}1^+CD8^+$ T cells did not correlate with disease-free survival (Extended Data Figure 8B), whereas to density of $CD39^+PD\text{-}1^+CD8^+$ T cells independent of their location did (Extended Data Figure 8C). In addition, we observed similar data when focusing on luminal A and B patients (Extended Data Figures 8D and 8E). The density of intra-tumoral $CD39^+PD\text{-}1^+CD8^+$ T cells was not an independent variable according to multivariate Cox regression analysis (Table 1). Importantly, the density of intra-tumoral $CD8^+$ T cells showed no correlation with disease-free survival (Figure 6C), strongly supporting our preclinical observations, namely that that disseminated cancer cells are controlled by this specific subset of $CD39^+PD\text{-}1^+CD8^+$ T cells.

Discussion

We discovered that breast cancer can prime a systemic, $CD8^+$ T cell response that mediates metastatic dormancy in the lungs and consequently, protects against clinical metastatic outgrowth. We thus describe an unexpected trait of primary tumors, in addition to their well-known metastasis-promoting capacity[25,26,45,46]. Using high-dimensional single-cell profiling of primary tumors, we identified the protective $CD8^+$ T cell population as PD-1^+ and $CD39^+$ cells, suggesting recent cognate interaction and tumor-specificity[20,47]. In line with our preclinical data, we found that a high density of intra-tumoral $CD39^+$PD-1^+CD8^+ T cells significantly correlated with disease-free survival after resection in breast cancer patients. Even in patients with luminal A or B subtypes, where the tumor tissue is generally less infiltrated by $CD8^+$ T cells[48], the presence of $CD39^+$PD-1^+CD8^+ T cells correlated with disease-free survival after primary tumor resection. As in our preclinical model, the heterogeneous population containing all $CD8^+$ T cells did not correlate with disease-free survival, strongly supporting the notion that $CD39^+$PD-1^+CD8^+ T cells comprise a population of cells that is uniquely equipped to control disseminated cancer cells.

We observed that $CD39^+$PD-1^+CD8^+ T cells express effector molecules but also markers that are typically associated with exhaustion. A similar population was recently described in human breast cancer[19,49]. Exhausted T cells are thought to have a reduced effector function and loss of proliferative capacity[50,51]. Nonetheless, exhausted T cells in breast cancer may be more functional than in melanoma[52].

In addition to local immunity, the induction of systemic immune responses by immunotherapy was shown to be essential for its efficacy[53], suggesting that protective $CD8^+$ T cells are recruited to the tumor. Recirculating $CD8^+$ T cells can also enter tissues, where they develop into $CD103^+$ tissue-resident memory cells and may protect tissues against disseminating tumor cells by the induction of cell death or cell cycle arrest[54]. Indeed, we detected $CD39^+PD\text{-}1^+CD8^+$ T cells in the primary tumor and in the lungs and found that a proportion expressed CD103 as a marker of tissue residency. It was recently shown that the presence of intra-tumoral CD103-expressing $CD8^+$ T cells correlate with survival in human breast cancer[41].

As mentioned above, metastatic dormancy may result from two different states[55]: Disseminated single cells that are quiescent[56], or micro-metastases that remain stable through an equilibrium between proliferation and death[57]. We found that disseminated 4T07 cells were present in the lungs as single non-cycling cells, suggesting dormancy through cell cycle arrest. Our observation that dormancy essentially depended on $CD8^+$ T cells uncovers a novel mechanism underlying dormancy. We found that protective $CD39^+PD\text{-}1^+CD8^+$ T cells produced TNFα and IFNγ, which were described to induce irreversible senescence in the context of Th1-mediated protection against cancer[42].

It may be that environmental cues induce cancer stem cell-like properties in disseminated cancer cells[58], which is in line with the low cycling frequency. Such cancer stem cells would represent a potent reservoir for progressive metastasis[59] in response to environmental changes. Why dormant cancer cells sometimes awaken only after decades[3] is still enigmatic, and it cannot be

excluded that different pathways converge to initiate growth of dormant lesions. Assuming $CD8^+$ T cells are required for maintenance of dormancy, it is conceivable that attrition of tissue-resident memory $CD8^+$ T cells may result in awakening of dormant cells. Tumor resection and consequent loss of antigen may result in diminished immunological memory; tissue-resident memory cells are described to be particularly unstable in the absence of antigen[60,61]. Alternatively, dormant cells themselves may change, for example losing the expression of molecules preventing immune-mediated clearance[62]. Finally, environmental factors in the broadest sense may awaken dormant cancer cells. Such changes in the microenvironment include fibrosis[63], tissue remodeling[64], obesity[65], inflammation[66], disturbance of vascular homeostasis[67], glucocorticoids[68], or cigarette smoke[69]. How such factors induce cycling of dormant cells and whether immune cells can interfere at this stage is unknown. Here we discovered that $CD39^+PD\text{-}1^+CD8^+$ T cells mediate dormancy of disseminated cancer cells but are by themselves unable to fully eradicate all of the cancer cells. This is clinically highly relevant, as dormant cancer cells are in all likelihood the source of future metastatic disease. Because the factors determining awakening are not known and may even not be controllable, it is important to better understand the nature of dormant cancer cells and which pathways must be mobilized for their complete elimination.

Acknowledgments

We thank Anne Müller, Lubor Borsig and Christian Münz (all University of

Zurich) for valuable input and support. We thank Fred Miller (Karmanos Cancer Institute) for providing cell lines. We thank the personnel from the Zurich Integrative Rodent Physiology (ZIRP, University of Zurich) and the Laboratory Animal Services Center (LASC, University of Zurich) for expert animal care. We thank Ruben Casanova (University of Zurich) for developing the R script converting immunofluorescence image data into file format compatible with flow cytometry data analysis software. This work was financially supported by the Swiss National Science Foundation (SNSF; CRSII5_177208 and 310030_175565 (MvdB), as well as 310030_170320, 310030_188450 and CRSII5_183478 (BB)), the Swiss Cancer League (Oncosuisse; KLS-4098-02-2017 (MvdB) and KFS-4431-02-2018 (BB)), the University of Zurich Forschungskredit (PTdL), the University Research Priority Program (URPP) Translational Cancer Research (MvdB, BB), the Science Foundation for Oncology (SFO; (MvdB)), the Helmut-Horten Foundation (MvdB), the Hartmann-Müller Foundation Zurich (MvdB), the Monique-Dornonville-de-la-Cour Foundation Zurich (MvdB) and the European Union H2020 Project iPC #826121 (BB).

Author contributions

PTdL, HCC and MvdB conceived experiments; PTdL, HCC, MV, NN, PC, EMC, VC, KS, FMA, JU, IG, MPL, SH performed and analyzed experiments; PTdL, HCC, BB and MvdB wrote the manuscript; BB, ST, BS and HM provided

essential reagents; BB helped with data analysis; PTdL and MvdB secured funding.

Declaration of interests

The authors declare no conflicting interests.

Methods

Mice

BALB/cJRj and BALB/cAnNRj-*Foxn1*$^{nu/nu}$ were purchased from Janvier labs (Roubaix, FR). NOD.Cg-*Prkdc*^{scid}*Il2rg*^{tm1Wjl}/SzJ mice were originally obtained from the Jackson Laboratory and provided by Christian Münz (University of Zurich, Switzerland). Mice were kept under specific pathogen-free conditions in individually ventilated cages at the Laboratory Animal Services Center at the University of Zurich. Mice had access to food and water *ad libitum* and were maintained on a 12-hour light/dark cycle with environmental enrichment. All experiments were performed with 8-14-weeks-old female mice in accordance with the Swiss federal and cantonal regulations on animal protection and were approved by The Cantonal Veterinary Office Zurich (156/2018).

Cell lines

4T07 and 4T1 cells were a gift from Fred Miller (Karmanos Cancer Institute, Detroit, USA). Cells were cultured in Dulbecco's Modified Eagle's Medium (DMEM, Gibco) supplemented with 10% fetal bovine serum (FBS, ThermoFisher Scientific), 2 mM L-glutamine and 2% penicillin/streptomycin (ThermoFisher Scientific). Cells were cultured at 37°C in a humidified atmosphere with 5% CO_2. 4T1 and 4T07 were lentivirally transduced to express firefly luciferase and ZsGreen (pHIV-Luc-ZsGreen, addgene plasmid #39196) or mCherry (pCDH-CMV-mCherry-T2A-Puro, addgene plasmid #72264).

Transduced cells were sorted based on expression of GFP or mCherry, respectively. Luciferase-ZsGreen is referred to as LZ, mCherry as mCh.

Only cells of early passages were used for experiments. Cells were regularly tested negative for mycoplasma by PCR analysis. Cells were also tested negative for 18 additional mouse pathogens by PCR (IMPACT II Test, IDEXX Bioanalytics).

In vivo tumor experiments and treatments

Hundred-thousand 4T1 or 4T07 cells in 50 μl PBS were injected into the fourth mammary fat pad. Alternatively, 3 x 10^5 cells in 50 μl PBS were injected into the lateral tail vein.

For resection of primary tumors, mice were anesthetized with 2.5 % isoflurane and given 0.04 mg/kg fentanyl (Kantonsapotheke Zurich) i.p. as pre-emptive analgesia. Primary tumors were resected, and wounds were closed using Autoclip wound clips (BD Biosciences). For post-operative analgesia 0.1 mg/kg buprenorphine (Temgesic, Schering-Plough) was given i.p. immediately after surgery and in the drinking water at 10 μg/ml for 48 hours ad libitum.

For depletion of $CD8^+$ T cells, 500 μg rat anti-mouse CD8 (clone YTS 169.4, hybridoma originally obtained from H. Waldmann, Oxford, United Kingdom) was injected intraperitoneally (i.p.) in PBS as described in each experiment. Control mice were injected with 500 μg rat anti-Trinitrophenol (clone 2A3, BioXCell). Antibodies were purified from hybridoma culture supernatant using protein G Sepharose 4 Fast Flow (Sigma). Injection of the respective antibody resulted in depletion of >90% of $CD4^+$ or $CD8^+$ T cells for at least 14 days, as

determined by flow cytometry. Antibodies were administered i.p. in 200 μl PBS. Full depletion of the targeted population was confirmed by flow cytometry on blood 2 d after injection of the antibody in every experiment.

Lung metastasis from luciferase- or mCherry-expressing tumors was quantified using an IVIS200 imaging system (PerkinElmer) as previously described[23]. Briefly, for luciferase-expressing tumors, mice were injected i.p. with 150 mg/kg D-luciferin (Promega) and photon flux was measured 20 minutes later in vivo as well as from dissected lungs. Lung metastasis from parental tumors was quantified by India Ink as previously described[23]. Briefly, mice were euthanized and India Ink (Pelikan, 15% in PBS) was injected intratracheally, lungs were harvested, washed in PBS and fixed in Fekete's solution (62% ethanol, 3.3% formaldehyde, 0.25 M acetic acid). Metastatic foci were counted blinded using a dissection microscope.

Disseminated cancer cells were detected in the lungs using a colony forming assay as previously described[21]. Briefly, lungs were resected from euthanized mice, cut into small pieces and digested for 45 minutes at 37°C in DMEM with 1 mg/ml collagenase IV and 2.6 μg/ml DNase I (both Sigma) on a rotating device. Subsequently, samples were washed with PBS by centrifugation at 350 *g*. For detection of circulating cancer cells, blood was collected by heart puncture in a 25-gauge syringe containing 100 µl heparin (5'000 IU/ml, Braun) and cells were washed with PBS by centrifugation at 350 *g*. Blood and lung samples were suspended in complete DMEM containing 6 μM of 6-thioguanine and cultured in a T175 flask. Medium was exchanged after 5-7 days and presence of colonies of tumor cells was evaluated after 14 days by light

microscopy and crystal violet staining.

Immunofluorescence of mouse samples

Organs were fixed with 4% paraformaldehyde (Roti-Histofix 4%, Roth) for 10 minutes at RT and cryoembedded in Optimal Cutting Temperature (O.C.T.) Compound (O.C.T.™ Compound, Tissue-Tek) using dry ice/100% ethanol slurry. Ten-*µ*m thick sections cut using a cryotome (Leica), mounted on SuperFrost glass slides, dried for 1h at 37°C and preserved at -80°C until immunostained. To prevent unspecific binding of antibodies, slides were incubated with 4% donkey serum in PBS (ANAWA BioWorld) for 10 minutes at RT. Subsequently, slides were incubated overnight at 4°C with primary antibody diluted in PBS 1% donkey serum. Following primary antibodies were used: Anti-mCherry (goat polyclonal antibody, AB8181-200 SICGEN, 1:400), Ki67 (rabbit monoclonal antibody, ab16667 abcam, 1:100). After incubation, slides were washed 3 times with PBS Tween 20 0.05% and incubated for 1 h at room temperature with secondary antibodies diluted in PBS 1% donkey serum. Following secondary antibodies were used: AF594-conjugated anti-goat IgG, AF488-conjugated anti-rabbit IgG (both Jackson ImmunoResearch, 1:400). Finally, slides were washed, incubated with 0.5 µg/ml 4′,6 diamidine-2-phenylindole (DAPI; Invitrogen) for 5 min, washed again and mounted with ProlongDiamond medium (Invitrogen). The slides were scanned using the automated multispectral microscopy system Vectra 3.0 (PerkinElmer). An unstained slide was used to generate the spectral profile of autofluorescence

in studied tissues. The Inform software (PerkinElmer) was used for spectral unmixing of individual fluorophores and autofluorescence.

Flow cytometry

Animals were euthanized by isoflurane overdose. The right heart ventricle was perfused with 10 ml PBS to eliminate the blood from the lung vessels. Primary tumors and lungs were collected in DMEM, cut into small pieces and digested for 45 minutes at 37°C in DMEM containing 1 mg/ml collagenase IV and 2.6 *µ*g/ml DNase I (both Sigma) on a rotating device. Samples were washed with PBS by centrifugation for 5 minutes at 350 *g*, the pellet was suspended in PBS and filtered through a 70-µm filter (BD Biosciences) to obtain a single cell suspension. For lymphocyte analysis, cells were further purified by centrifugation over a Percoll gradient (GE Healthcare, 17-0891-01, Sigma Aldrich).

Single cells were stained according to standard protocols. Briefly, cells were surface-stained in 50 *µ*l antibody-mix in PBS. For intracellular cytokine staining, cells were stimulated with 100 ng/ml phorbol 12-myristate 13-acetate (PMA) plus 1 *µ*g/ml ionomycin for 4 h at 37°C in the presence of GolgiPlug/GolgiStop (BD Pharmigen). Cells were stained for surface molecules as described above, washed with PBS, and fixed for 30 min on ice using IC Fixation Buffer from Foxp3/Transcription Factor Staining Buffer Set (eBioscience). Subsequently, cells were stained for intracellular cytokines in permeabilization buffer from the Foxp3/Transcription Factor Staining Buffer Set overnight at 4°C. After washing with permeabilization buffer, samples were suspended in FACS buffer (PBS,

20 mM EDTA pH 8.0, 2% FCS) and acquired using a CyAn ADP9 flow cytometer (Beckman Coulter), FACS LSRII Fortessa or FACSymphony (both BD Biosciences). For quantitative analysis, CountBright absolute counting beads were used (ThermoFisher Scientific). In all staining, dead cells were excluded using Live/Dead fixable staining reagents (Invitrogen), and doublets were excluded by FSC-A versus FSC-H and SSC-A versus SSC-H gating. Following directly labelled primary antibodies were used: Anti-CD8 in BUV 805, clone 53-6.7, rat IgG2a, BD Pharmingen. Anti-CD11b in BUV 661, clone M1/70, rat IgG2b, BD Pharmingen. Anti-CD45.2 in BUV 653, clone 30-F11, rat IgG2b, BD Pharmingen. Anti-VISTA in AF488, clone MH5A, armenian hamster IgG1, BioLegend. Anti-CD39 in PerCP-eFluor710, clone 24DMS1, rat IgG2b, ThermoFisher Scientific. Anti-LAG3 in BV 421, clone C9B7W, rat IgG1, BioLegend. Anti-CD44 in BV 570, clone IM7, rat IgG2b, BioLegend. Anti-CD73 in BV 605, clone TY/11.8, rat IgG1, BioLegend. Anti-CD25 in BV 650, clone PC61, rat IgG1, BioLegend. Anti-PD-1 in BV 785, clone 29F.1A12, rat IgG2a, BioLegend. Anti-TCRβ in PE-Cy5, clone H57-597, armenian hamster IgG1, BioLegend. Anti-KLRG1 in APC-Cy7, clone 2F1/KLRG1, armenian hamster IgG1, BioLegend. Anti-TIM3 in AF647, clone B8.2C12, rat IgG1, BioLegend. Anti-CD103 in Biotin, clone 2E7, armenian hamster IgG1, BioLegend. Anti-Streptavidin in BUV 395, BD Pharmingen. Anti-Ki67 in BV 480, clone B56, mouse IgG1, BD Pharmingen. Anti-TNFα in BV711, clone MP6-XT22, rat IgG1, BioLegend. Anti-INFγ BUV 737, clone XMG1.2, rat IgG1, BD Pharmingen. Anti-CD4 in BUV 496, clone GK1.5, rat IgG2b, BD Pharmingen. Anti-FOXP3 in PE, clone FJK-16s, rat IgG2a, ThermoFisher Scientific. Anti-EOMES in PE-

eFluor610, clone Dan11mag, rat IgG2a, ThermoFisher Scientific. Anti-T-bet in PE-Cy7, clone eBio4B10, rat IgG1, ThermoFisher Scientific. Anti-CTLA4 in APC-AR700, clone UC10-4F10-11, armenian hamster IgG1, BD Pharmingen. Flow cytometry data were compensated and exported using FlowJo software (version 10, TreeStar Inc.). The exported FCS files were normalized using Cyt3 MATLAB (version 2017b) and uploaded into Rstudio (R software environment, version 3.4.0). tSNE and FlowSOM algorithm mapping live cells from a pooled sample were performed as described[70]. CellCNN was run using default parameters, dividing data into training and validation steps as described[33].

Purification of CD39$^+$PD-1$^+$CD8$^+$ T cells

Primary tumors were processed as described under “Flow Cytometry”. After the Percoll gradient, the leukocyte fraction was enriched for CD8$^+$ T cells using anti-mouse CD8a microbeads (Miltenyi Biotec) and autoMACS equipment (Miltenyi Biotec) according to the manufacturer’s instructions. Subsequently, cells were stained for CD39, PD-1 and CD8 as described under “Flow Cytometry” and live, single CD39$^+$PD-1$^+$CD8$^+$ T cells as well as other CD8$^+$ T cells were sorted using an ARIA III Sorter (BD Biosciences).

Adoptive transfer of CD39$^+$PD-1$^+$CD8$^+$ T cells

Sorted cells were counted using trypan blue (Trypan Blue solution, Sigma Aldrich) to exclude dead cells. Two-hundred-thousand CD39$^+$PD-1$^+$CD8$^+$ T cells were injected immediately after 10^5 4T07-LZ cells. Injections were given intravenously.

In vitro induction of senescence

Twenty-thousand 4T07 cells were plated in a 6-well plate. Subsequently, 75 ng/ml mouse IFNγ (R&D Systems) plus 5 ng/ml mouse TNFα (PeproTech) were added and cells were incubated at 37°C in a humidified atmosphere with 5% CO_2 for 6 days as described. The proportion of senescent cells was determined by staining for β-galactosidase activity using Senescence β-Galactosidase Staining Kit (9860, Cell Signaling Technology) as described[42].

RNA-sequencing

Library preparation: The libraries were prepared following the Smart-seq2 protocol[71]. Five-hundred pg of cDNA from each sample were tagmented and amplified using Illumina Nextera XT kit. The resulting libraries were pooled, double-sided size selected (0.5x followed by 0.8x ratio using Beckman Ampure XP beads) and quantified using an Agilent 4200 TapeStation System. The pool of libraries was sequenced in an Illumina NovaSeq6000 sequencer (single-end 100 bp) with a depth of around 20 Mio reads per sample as a service by the Functional Genomics Center Zurich (FGCZ).

Data evaluation: The raw data generated by Illumina NovaSeq6000 sequencer were analyzed using SUSHI, a framework for analysis of NGS data developed by the FGCZ (Hatakeyama et al., 2016, Qi et al., 2017). Briefly, after quality control, the reads were aligned to a reference genome (Ensembl genome Mus_musculus. GRCm38 dated 2018.02.26) with STAR 2.7.3a. The software package EdgeR was used to detect differentially expressed genes. We applied

a threshold of $p < 0.01$ and adjusted $p<0.1$ (i.e., FDR<2%). Unsupervised hierarchical clustering was done using the Ward2 method. Heatmaps were generated with the software FunRich V3.1.3.

Gene set enrichment analysis[43,72] was performed on a list of genes ranked from high to low estimated fold-change using the GSEA 4.0.3 Software (Broad Institute) with enrichment statistic classic and 1000 permutations.

Patient material

Tumor tissues from 54 patients with breast cancer (Table 1) were collected at the University Hospital Zurich, Switzerland. Donors provided written, informed consent to tissue collection, analysis and data publication according to the Declaration of Helsinki. Law abidance was reviewed and approved by the ethics commission of the Canton Zurich (BASEC-Nr. 2018-02282 and KEK-ZH-2013-0584). Samples were numerically coded to protect donors' rights to confidentiality and privacy.

Immunofluorescence of human samples

Formalin-fixed paraffin-embedded samples were cut into 2 μm-thick sections and dried overnight at 55°C. Antigen retrieval and deparaffinization were performed in 1x Trilogy Solution (Cell Marque, 920P-06) for 15 minutes at 115°C. Staining was performed employing tyramide signal amplification (TSA) and the Opal™ 7-color Manual IHC Kit (PerkinElmer). To prevent unspecific binding of antibodies, slides were incubated with 4% donkey serum in PBS (ANAWA BioWorld) in PBS/0.1% Triton X-100 for 15 minutes at 37°C. TSA

staining protocol was performed as described[73]. Briefly, slides were incubated overnight at 4°C with primary antibody diluted in PBS/1% donkey serum/0.1% Triton X-100. Subsequently, slides were washed in PBS Triton X-100 0.1% and incubated with corresponding HRP-conjugated secondary antibodies. Following primary antibodies were used: Anti-CD39 (mouse monoclonal antibody, clone A1, BioLegend, 1:500), anti-PD-1 (rabbit monoclonal antibody, clone D4W2J BioConcept, 1:4000), anti-CD8 (mouse monoclonal antibody, clone RPA-T8, Cell Signaling, 1:2000), anti-PAN-Cytokeratin (rabbit polyclonal antibody, cat. no. H-240, Santa Cruz, 1:2000) and anti-EpCAM (rabbit monoclonal antibody, clone EPR20532-225, Abcam, 1:200). Following HRP-conjugated secondary antibodies were used: anti-mouse IgG (H+L) (donkey polyclonal antibody, 715-035-151 Jackson ImmunoResearch 1:500) and anti-rabbit IgG (H+L) (donkey polyclonal antibody, 715-035-152 Jackson ImmunoResearch 1:1000). Fluorescent signal was developed using the Opal™ 7-color Manual IHC Kit. Finally, slides were washed, incubated with 0.5 μg/ml 4′,6-diamidine-2-phenylindole (DAPI; Invitrogen) for 5 min, washed again and mounted with ProlongDiamond medium (Invitrogen). The slides were scanned using the automated multispectral microscopy system Vectra 3.0 (PerkinElmer). An unstained slide was used to generate the spectral profile of autofluorescence in studied tissues. The Inform software (PerkinElmer) was used for (i) unmixing the spectra of individual fluorophores and autofluorescence, (ii) performing automated tissue and cell segmentation into tumor and non-tumor cells, and (iii) exporting single-cell intensity values for all fluorescent signals. Single-cell parameter files were transformed into .fcs files

using R script (version 3.6.1) involving FlowCore and Biobase packages and were analyzed using FlowJo software to gate on $CD39^+PD\text{-}1^+CD8^+$ T cell populations in tumor tissue category (Extended Data Figure 8F). Gates were set based on the intensity values identified in the fluorescent images. Cell density values were measured as number of cells/mm^2 obtained as cell counts from the gated populations divided by the tumor tissue area measured in the corresponding patient. Samples were analyzed blinded.

Statistical analysis

Data were analyzed using GraphPad Prism 8.0 for Windows or Mac, and RStudio (version 1.2.5019). For comparison of 2 experimental groups, 2-tailed Student's t test with Welch's correction was performed. More than 2 groups were compared using an ANOVA test with Bonferroni's correction. Data following a logarithmic distribution (i.e. IVIS signal) were log transformed prior to analysis. The number of mice per experimental group was determined based on our previous experience with similar models. Every point represents one mouse. Unless stated otherwise, data are shown as mean ± SD. $p < 0.05$ is considered significant throughout. $^*p < 0.05$, $^{**}p < 0.01$, $^{***}p < 0.001$, $^{****}p < 0.0001$.

Density of $CD39^+PD\text{-}1^+CD8^+$ T cells was correlated with the clinicopathological information of the patients using corresponding R packages. Disease-free survival was analyzed by Kaplan-Meier curve and log-rank test (Survminer and Survival R packages), as well as univariate and multivariate Cox regression (pROC, ROCR and Survival R packages). The threshold of $CD39^+PD\text{-}$

1^{+}CD8^{+} or CD8^{+} T cell density was identified by the Receiver Operating Characteristics (ROC) curve analysis using 3-year disease-free survival for defining long- and short-term survivors. Following values apply: Intra-tumoral CD39^{+}PD-1^{+}CD8^{+} T cells, 4.20; extra-tumoral CD39^{+}PD-1^{+}CD8^{+} T cells, 8.43; total CD39^{+}PD-1^{+}CD8^{+} T cells, 5.71; intra-tumoral CD8^{+} T cells, 249.20; extra-tumoral CD8^{+} T cells, 1218.60; total CD8^{+} T cells, 562.29.

Data deposition

https://www.ncbi.nlm.nih.gov/sra/PRJNA609233

Legends to the figures

Figure 1. 4T07 but not 4T1 breast cancer cells are dormant after dissemination to the lungs.

(A) Diagram of the origin of 4T1 and 4T07 cell lines[21]. **(B)** Experimental design. 4T1 or 4T07 cells (10^5) were injected into the mammary fat pad of female BALB/c mice. Analysis was performed 30 d later. **(C)** Growth curve of primary breast cancer. **(D)** Representative pictures of lungs at the endpoint stained with India ink to visualize metastatic nodules (left panels). The number of metastatic foci in the lungs (right panel). **(E)** 4T07-mCh cells (10^5) were injected into the mammary fat pad of female BALB/c mice. Analysis was performed 35 d later. Representative section of the primary tumor (upper panels) and lung (lower panels) at the endpoint. Disseminated 4T07 cells were detected as single, Ki67-negative cells in the lungs of 5 out of 5 mice. Disseminated 4T07 cells are shown in red, Ki67 in green, DAPI in blue. Scale bar indicates 50 μm. **(F)** Experimental design. 4T1 or 4T07 cells (10^5) were injected into the mammary fat pad of female BALB/c mice. The tumor was resected 20 d after injection and analysis was performed 21 d after resection (endpoint). **(G)** Representative section of the lung at the endpoint. Disseminated 4T07 cells were detected as single, Ki67-negative cells in the lungs of 5 out of 5 mice. Disseminated 4T07 cells are shown in red, Ki67 in green, DAPI in blue. Scale bar indicates 20 μm. Each symbol represents an individual mouse. Five mice per group. *$p < 0.05$, ***$p < 0.001$ (2-tailed Student's t-test). The bar represents the mean ± SD. Results are representative of 3 independent experiments.

Figure 2. Induction of protective immunity by the primary tumor mediates metastatic dormancy.

(A) Experimental design. 4T1 or 4T07 cells ($3x10^5$) were injected i.v. into female BALB/c mice. Analysis was performed 25 d later. **(B)** Metastatic load in the lungs determined by counting nodules. **(C)** Experimental design. 4T1 or 4T07 cells (10^5) were injected into the mammary fat pad of female BALB/c (*n*=5) or BALB/c *Foxn1*$^{nu/nu}$ (*n*=7) mice. Analysis was performed 30 d later. Lungs of "WT Late" mice (*n*=4) were analyzed when the 4T07 tumor size reached the size of the BALB/c *Foxn1*$^{nu/nu}$ group, e.g. 35 days after tumor cell injection. **(D)** Weight of primary tumors. Left panel with closed symbols, 4T1; right panel with open symbols, 4T07. **(E)** Metastatic load in the lungs determined by counting nodules. Left panel with closed symbols, 4T1; right panel with open symbols, 4T07. **(F)** Experimental design. Female BALB/c mice received 0.5 mg anti-CD8 or isotype control i.p. and 1 d later 10^5 4T07-mCh cells in the mammary fat pad. Analysis was performed 25 d later. **(G)** Metastatic load in the lungs measured by bioluminescence. **(H)** Bioluminescence images. **(I)** Experimental design. 4T07 cells (10^5) or PBS were injected into the mammary fat pad of female BALB/c mice on d 0. On d 11, $3x10^5$ 4T07-LZ cells were injected i.v. and analysis of lung metastatic load was performed on d 25. **(J)** Quantification of lung metastatic load by bioluminescence. **(K)** Bioluminescence images.

Each symbol represents an individual mouse. *$p < 0.05$, **$p < 0.01$, ****$p < 0.0001$, ns = not significant (2-tailed Student's t-test with Welch's correction (B, D left panel, E left panel, G, J), ANOVA with Bonferroni correction (D right

panel, E right panel). The bar represents the mean ± SD. Results are representative of at least 2 independent experiments.

Figure 3. CD39$^+$PD-1$^+$CD8$^+$ T cells emerge in dormant breast cancer. Female BALB/c mice were injected with 10^5 4T1 or 4T07 cells in the mammary fat pad and primary tumors were analyzed by flow cytometry 20 d later (*n*=4). **(A)** t-SNE visualization of markers after gating on single, live, CD45$^+$ TCRβ$^+$ cells. **(B)** Upper panel: t-SNE plots of the main T cell subsets. Lower left panel: Frequency of the main T cell subsets in both groups. Each symbol represents an individual mouse. Lower right panel: Heat map with marker expression of the main T cell subsets. **(C)** t-SNE visualization of markers on CD8$^+$ TCRβ$^+$ cells. **(D)** Upper panel: t-SNE plots of the main CD8$^+$ T cell subsets identified by FlowSOM algorithm. Lower panel: Frequency of the main CD8$^+$ T subsets identified by FlowSOM algorithm in both groups. **(E)** Scaled histograms of arcsinh-transformed marker expression showing the relative marker distribution of the population identified by CellCnn (red) among all CD8$^+$ T cells (blue). KS indicates the Kolmogorov–Smirnov two-sample test between the whole-cell population and the selected cell subsets. **(F)** Heat map with marker expression of the main CD8$^+$ T cell subsets identified by FlowSOM algorithm. **(G)** Representative FACS plot of 4T1 and 4T07 primary tumors after gating on CD8$^+$ TCRβ$^+$. **(H)** Frequency of the population of total CD8$^+$ identified by CellCnn in both models. **(I)** The number of CD39$^+$PD-1$^+$CD8$^+$ T cells in the lungs. **(J)** Representative CD103-staining of live CD39$^+$PD-1$^+$CD8$^+$ T cells from the lungs.

Each symbol represents an individual mouse. *$p < 0.05$, ****$p < 0.0001$ (2-tailed Student's t-test with Welch's correction). The bar represents the mean ± SD.

Figure 4. Tumor-associated CD39$^+$PD-1$^+$CD8$^+$ T cells prevent metastatic outgrowth.

(A) Gating used for sorting of CD39$^+$PD-1$^+$CD8$^+$ and the rest of the CD8$^+$ population (termed other CD8$^+$ T cells) from established 4T07 orthotopic breast tumors. **(B)** Experimental design. Two-hundred-thousand sorted CD39$^+$PD-1$^+$CD8$^+$ or other CD8$^+$ T cells were transferred after injection of 10^5 4T07-LZ cells into female BALB/c mice. All injections were given intravenously. Lung metastatic load was determined by bioluminescence 14 d later. **(C)** Bioluminescence of lungs at endpoint. **(D)** Quantification of lung metastatic load by bioluminescence.

Each symbol represents an individual mouse. Five mice per group. **$p < 0.01$, ***$p < 0.001$ (ANOVA with Bonferroni's correction). The bar represents the mean ± SD.

Figure 5. CD39$^+$PD-1$^+$CD8$^+$ T cells have a unique transcriptional signature.

(A) Hierarchical clustering of gene expression by sorted CD39$^+$PD-1$^+$CD8$^+$ and CD8$^+$ T cells. **(B)** Volcano plot comparing transcripts in CD39$^+$PD-1$^+$CD8$^+$ T cells with those in other CD8$^+$ T cells sorted from 4T07 breast tumors. The red symbols represent transcripts that are significantly over-expressed in CD39$^+$PD-1$^+$CD8$^+$ T cells, whereas the blue symbols represent significantly under-expressed transcripts. **(C)** Heat map showing relative expression of

selected transcripts in CD39$^+$PD-1$^+$CD8$^+$ (three top rows) and other CD8$^+$ T cells (three bottom rows) identified by differential gene expression analysis. **(D)** Gene set enrichment analysis comparing the transcriptional profile to the data published by Goldrath et al.[74] et al (left panel) and Savas et al.[19] (right panel).

Figure 6. High density of intra-tumoral CD39$^+$PD-1$^+$CD8$^+$ but not total CD8$^+$ T cells correlates with disease-free survival in human breast cancer.

(A) Representative images of 5-color multiplex immunofluorescence on human breast cancer. Staining shows epithelial cells (PanCK + EpCAM, yellow), CD8$^+$ T cells (CD8, magenta), PD-1 (green), CD39 (red) and nuclear staining (DAPI, blue). Scale bar is 50 µm. **(B)** Disease-free survival of 54 patients with high or low number of intra-tumoral CD39$^+$PD-1$^+$CD8$^+$ T cells**. (C)** Disease-free survival of 54 patients with high or low number of intra-tumoral CD8$^+$ T cells. The threshold for separating patients with high and low CD39$^+$PD-1$^+$CD8$^+$ T cell densities was defined using ROC curve analysis.

Legends to the extended data figures

Extended Data Figure 1. Circulating and disseminated cancer cells in mice with 4T1 or 4T07 orthotopic tumors.

(A) BALB/c mice were injected with 10^5 4T1 or 4T07 cells in the mammary fat pad and disseminated cancer cells (DCCs) were detected by colony-forming assay in lungs 30 d later. DCCs were detected in all mice (n=5 per group). Representative images of colonies from cultured lung-digests are shown. **(B)** 4T07-mCh cells (10^5) were injected into the mammary fat pad of female BALB/c mice. Analysis was performed 35 d later. Disseminated 4T07 cells were found in 5/5 mice and are shown in red, Ki67 in green, DAPI in blue. Representative pictures from a cohort of 5 mice. Scale bar: 20 μm.

Results are representative of 3 independent experiments.

Extended Data Figure 2. 4T07 and 4T1 induce similar systemic inflammation.

Female BALB/c mice were injected with 10^5 4T1 or 4T07 cells in the mammary fat pad. Control mice were injected with PBS. Analysis was performed at the indicated days after cancer cell injection. **(A)** Spleen weight. **(B)** Percentage circulating neutrophils of $CD45^+$ cells. **(C-F)** Total number of cells per mg lung tissue: inflammatory monocytes (C), neutrophils (D), eosinophils (E), alveolar macrophages (F). **(G)** Female BALB/c mice were injected with 10^5 4T1 cells into the mammary fat pad. The plots show a representative gating strategy of lungs processed 20 d after tumor cell injection.

Each symbol represents an individual mouse. Five mice per group. ns = not significant (2-tailed Student's t-test with Welch's correction). The bar represents the mean ± SD.

Extended Data Figure 3. 4T07 breast cancer elicits systemic protective immunity.

(A) Experimental design. 4T07 cells (10^5) or PBS were injected into the mammary fat pad of female BALB/c mice on d 0. On d 11, 10^5 4T07-mCh cells were injected i.v. and analysis of lung metastatic load was performed on d 25. **(B)** Representative section of the lung at the endpoint. Disseminated 4T07 cells were detected as single, Ki67-negative cells in the lungs of 5 out of 5 mice. Disseminated 4T07 cells are shown in red, DAPI in blue. Scale bar indicates 20 μm. **(C)** Experimental design. 4T07 cells (10^5) or PBS were injected into the mammary fat pad of female BALB/c mice on d 0. The tumor was resected on d 8 (PBS-injected mice underwent mock surgery) and $3x10^5$ 4T07-LZ cells were i.v. injected on d 15. The lung metastatic load was quantified on d 30. **(D)** Quantification of lung metastatic load by bioluminescence. ****$p < 0.0001$, (2-tailed Student's t-test with Welch's correction). The bar represents the mean ± SD. Each symbol represents an individual mouse. The bar represents the mean ± SD. Results are representative of 2 independent experiments. **(E)** 4T07 cells (10^5) or PBS were injected into the mammary fat pad of female BALB/c mice on d 0. On day 8, mice were injected i.p. with 500 μg anti-CD8 or isotype control. On d 15, $3x10^5$ 4T07-LZ cells were i.v. injected and lung metastatic load was quantified on d 25. **(F)** Quantification of the lung metastatic load by

bioluminescence on d 25. ****$p < 0.0001$ (ANOVA test with Bonferroni's correction). Each symbol represents an individual mouse. The bar represents the mean ± SD. Results are representative of 2 independent experiments. **(G)** Experimental design. 4T1 cells (10^5) or PBS were injected into the mammary fat pad of female BALB/c mice on d 0. On d 11, $3x10^5$ 4T1-LZ cells were injected and analysis of lung metastatic load was performed on d 25. **(H)** Quantification of lung metastatic load by bioluminescence. ns = not significant (2-tailed Student's t-test with Welch's correction). Each symbol represents an individual mouse. The bar represents the mean ± SD.

Extended Data Figure 4. Gating and quantification of tumor-associated leukocytes.

4T07 cells (10^5) or PBS were injected into the mammary fat pad of female BALB/c mice and tumors were processed for flow cytometry 20 d later. **(A)** Gating strategy. **(B-F)** Total number of cells per mg tumor tissue: (B) eosinophils, (C) neutrophils, (D) NK cells, (E) inflammatory monocytes, (F) macrophages. Each symbol represents an individual mouse. Six (4T07) or seven (4T1) mice per group. ****$p < 0.0001$ (2-tailed Student's t-test with Welch's correction). The bar represents the mean ± SD.

Extended Data Figure 5. Expression of selected markers by $CD39^+PD-1^+CD8^+$ T cells.

Female BALB/c mice were injected with 10^5 4T1 or 4T07 cells in the mammary fat pad and primary tumors were analyzed by flow cytometry 20 d later (n=4).

(A) Gating strategy for Figure 3. **(B)** Representative examples of expression of selected markers on live, single $CD45^+TCR\beta^+CD11b^-CD39^+PD\text{-}1^+CD8^+$ T cells.

Extended Data Figure 6. IFNγ and TNFα induce senescence of 4T07 cells. Twenty-thousand 4T07 cells were plated in a 6-well plate. Subsequently, 75 ng/ml mouse IFNγ plus 5 ng/ml mouse TNFα were added and cells were incubated for 6 days. **(A)** Proportion of senescent cells in control and IFNγ plus TNFα-exposed 4T07 cells. Each symbol represents an individual culture. $^{**}p < 0.01$ (2-tailed Student's t-test with Welch's correction). The bar represents the mean ± SD. Results are representative of 2 independent experiments. **(B)** Representative examples of staining for SA-β-galactosidase activity (blue) as proxy for senescence. Left panel, medium. Right panel, IFNγ plus TNFα.

Extended Data Figure 7. $CD39^+PD\text{-}1^+CD8^+$ T cells in dormant and metastatic tumors have a similar transcription signature.

(**A)** Volcano plot comparing transcripts in $CD39^+PD\text{-}1^+CD8^+$ T cells sorted from 4T07 breast tumors with those sorted from 4T1 breast tumors. The red symbols represent transcripts that are significantly overexpressed in $CD39^+PD\text{-}1^+CD8^+$ T cells from 4T07 breast tumors, whereas the blue symbols represent significantly underexpressed transcripts.

Extended Data Figure 8. High density of intra-tumoral $CD39^+PD\text{-}1^+CD8^+$ but not total $CD8^+$ T cells correlate with disease-free survival in human luminal A and B breast cancer.

(A) Disease-free survival of patients with luminal A, luminal B or triple-negative (TN) breast cancer. **(B)** Disease-free survival of 54 patients with high or low number of extra-tumoral $CD39^+PD\text{-}1^+CD8^+$ T cells. **(C)** Disease-free survival of 54 patients with high or low number of intra-tumoral + extra-tumoral $CD39^+PD\text{-}1^+CD8^+$ T cells. **(D)** Disease-free survival of 20 luminal A and 25 luminal B breast cancer patients with high or low number of intra-tumoral $CD39^+PD\text{-}1^+CD8^+$ T cells**.** **(E)** Disease-free survival of 20 luminal A and 25 luminal B breast cancer patients with high or low number of intra-tumoral $CD8^+$ T cells**.** ns = not significant. **(F)** Representative example of a sample with high (upper panels) or low (lower panels) number of intra-tumoral $CD39^+PD\text{-}1^+CD8^+$ T cells. Single-cell parameter files were transformed into .fcs files using R studio and were analyzed using FlowJo software. Values of number of cells/mm^2 were obtained by using the values of total counts obtained from the FlowJo analysis and the measurements of tumor tissue area obtained from the inform analysis. The threshold for separating patients with high and low $CD39^+PD\text{-}1^+CD8^+$ T cell densities was defined using ROC curve analysis.

1. Kennecke, H. *et al.* Metastatic behavior of breast cancer subtypes. *J. Clin. Oncol.* (2010). doi:10.1200/JCO.2009.25.9820
2. Colzani, E. *et al.* Time-dependent risk of developing distant metastasis in breast cancer patients according to treatment, age and tumour characteristics. *Br. J. Cancer* (2014). doi:10.1038/bjc.2014.5
3. Pan, H. *et al.* 20-year risks of breast-cancer recurrence after stopping endocrine therapy at 5 years. *N. Engl. J. Med.* (2017). doi:10.1056/NEJMoa1701830
4. Karrison, T. G., Ferguson, D. J. & Meier, P. Dormancy of mammary carcinoma after mastectomy. *J. Natl. Cancer Inst.* (1999). doi:10.1093/jnci/91.1.80
5. Demicheli, R., Abbattista, A., Miceli, R., Valagussa, P. & Bonadonna, G. Time distribution of the recurrence risk for breast cancer patients undergoing mastectomy: Further support about the concept of tumor dormancy. *Breast Cancer Res. Treat.* (1996). doi:10.1007/BF01807163
6. Sosa, M. S., Bragado, P. & Aguirre-Ghiso, J. A. Mechanisms of disseminated cancer cell dormancy: an awakening field. *Nat Rev Cancer* **14**, 611–622 (2014).
7. Braun, S. *et al.* A pooled analysis of bone marrow micrometastasis in breast cancer. *N. Engl. J. Med.* (2005). doi:10.1056/NEJMoa050434
8. Janni, W. *et al.* Persistence of disseminated tumor cells in the bone marrow of breast cancer patients predicts increased risk for relapse - A European pooled analysis. *Clin. Cancer Res.* (2011). doi:10.1158/1078-0432.CCR-10-2515

9. Balz, L. M. *et al.* The interplay of HER2/HER3/PI3K and EGFR/HER2/PLC-γ1 signalling in breast cancer cell migration and dissemination. *J. Pathol.* (2012). doi:10.1002/path.3991

10. Ranganathan, A. C., Zhang, L., Adam, A. P. & Aguirre-Ghiso, J. A. Functional coupling of p38-induced up-regulation of BiP and activation of RNA-dependent protein kinase-like endoplasmic reticulum kinase to drug resistance of dormant carcinoma cells. *Cancer Res.* (2006). doi:10.1158/0008-5472.CAN-05-3092

11. Ghajar, C. M. Metastasis prevention by targeting the dormant niche. *Nature Reviews Cancer* (2015). doi:10.1038/nrc3910

12. Ghajar, C. M. *et al.* The perivascular niche regulates breast tumour dormancy. *Nat Cell Biol* **15**, 807–817 (2013).

13. Bragado, P. *et al.* TGF-β2 dictates disseminated tumour cell fate in target organs through TGF-β-RIII and p38α/β signalling. *Nat. Cell Biol.* (2013). doi:10.1038/ncb2861

14. Hagerling, C. *et al.* Immune effector monocyte–neutrophil cooperation induced by the primary tumor prevents metastatic progression of breast cancer. *Proc. Natl. Acad. Sci. U. S. A.* (2019). doi:10.1073/pnas.1907660116

15. Malladi, S. *et al.* Metastatic Latency and Immune Evasion through Autocrine Inhibition of WNT. *Cell* **165**, 45–60 (2016).

16. Eyles, J. *et al.* Tumor cells disseminate early, but immunosurveillance limits metastatic outgrowth, in a mouse model of melanoma. *J Clin Invest* **120**, 2030–2039 (2010).

17. Pommier, A. *et al.* Unresolved endoplasmic reticulum stress engenders immune-resistant, latent pancreatic cancer metastases. *Science (80-.).* (2018). doi:10.1126/science.aao4908

18. Ali, H. R. *et al.* Association between CD8+ T-cell infiltration and breast cancer survival in 12 439 patients. *Ann. Oncol.* (2014). doi:10.1093/annonc/mdu191

19. Savas, P. *et al.* Single-cell profiling of breast cancer T cells reveals a tissue-resident memory subset associated with improved prognosis. *Nat. Med.* (2018). doi:10.1038/s41591-018-0078-7

20. Simoni, Y. *et al.* Bystander CD8 + T cells are abundant and phenotypically distinct in human tumour infiltrates. *Nature* (2018). doi:10.1038/s41586-018-0130-2

21. Aslakson, C. J. & Miller, F. R. Selective events in the metastatic process defined by analysis of the sequential dissemination of subpopulations of a mouse mammary tumor. *Cancer Res* **52**, 1399–1405 (1992).

22. Pulaski, B. A. & Ostrand-Rosenberg, S. Mouse 4T1 Breast Tumor Model. in *Current Protocols in Immunology* (2001). doi:10.1002/0471142735.im2002s39

23. Beffinger, M. *et al.* CSF1R-dependent myeloid cells are required for NKmediated control of metastasis. *JCI Insight* **3**, (2018).

24. Carlson, P. *et al.* Targeting the perivascular niche sensitizes disseminated tumour cells to chemotherapy. *Nat. Cell Biol.* (2019). doi:10.1038/s41556-018-0267-0

25. Peinado, H. *et al.* Pre-metastatic niches: organ-specific homes for

metastases. *Nat Rev Cancer* **17**, 302–317 (2017).

26. Spiegel, A. *et al.* Neutrophils Suppress Intraluminal NK Cell-Mediated Tumor Cell Clearance and Enhance Extravasation of Disseminated Carcinoma Cells. *Cancer Discov* **6**, 630–649 (2016).

27. Kowanetz, M. *et al.* Granulocyte-colony stimulating factor promotes lung metastasis through mobilization of Ly6G+Ly6C+ granulocytes. *Proc Natl Acad Sci U S A* **107**, 21248–21255 (2010).

28. Ouzounova, M. *et al.* Monocytic and granulocytic myeloid derived suppressor cells differentially regulate spatiotemporal tumour plasticity during metastatic cascade. *Nat. Commun.* (2017). doi:10.1038/ncomms14979

29. Sharma, S. K. *et al.* Pulmonary Alveolar Macrophages Contribute to the Premetastatic Niche by Suppressing Antitumor T Cell Responses in the Lungs. *J. Immunol.* (2015). doi:10.4049/jimmunol.1403215

30. Van Der Maaten, L. & Hinton, G. Visualizing data using t-SNE. *J. Mach. Learn. Res.* (2008).

31. Van Gassen, S. *et al.* FlowSOM: Using self-organizing maps for visualization and interpretation of cytometry data. *Cytom. Part A* (2015). doi:10.1002/cyto.a.22625

32. Weber, L. M. & Robinson, M. D. Comparison of clustering methods for high-dimensional single-cell flow and mass cytometry data. *Cytom. Part A* (2016). doi:10.1002/cyto.a.23030

33. Arvaniti, E. & Claassen, M. Sensitive detection of rare disease-Associated cell subsets via representation learning. *Nat. Commun.*

(2017). doi:10.1038/ncomms14825

34. Krieg, C. *et al.* High-dimensional single-cell analysis predicts response to anti-PD-1 immunotherapy. *Nat Med* **24**, 144–153 (2018).

35. Anderson, A. C., Joller, N. & Kuchroo, V. K. Lag-3, Tim-3, and TIGIT: Co-inhibitory Receptors with Specialized Functions in Immune Regulation. *Immunity* **44**, 989–1004 (2016).

36. Pandiyan, P., Hegel, J. K. E., Krueger, M., Quandt, D. & Brunner-Weinzierl, M. C. High IFN-γ Production of Individual CD8 T Lymphocytes Is Controlled by CD152 (CTLA-4). *J. Immunol.* **178**, 2132–2140 (2007).

37. Workman, C. J. *et al.* Lymphocyte Activation Gene-3 (CD223) Regulates the Size of the Expanding T Cell Population Following Antigen Activation In Vivo. *J. Immunol.* **172**, 5450–5455 (2004).

38. Koyama, S. *et al.* Adaptive resistance to therapeutic PD-1 blockade is associated with upregulation of alternative immune checkpoints. *Nat. Commun.* **7**, 1–9 (2016).

39. Clarke, J. *et al.* Single-cell transcriptomic analysis of tissue-resident memory T cells in human lung cancer. *J. Exp. Med.* (2019). doi:10.1084/jem.20190249

40. Park, C. O. & Kupper, T. S. The emerging role of resident memory T cells in protective immunity and inflammatory disease. *Nature Medicine* (2015). doi:10.1038/nm.3883

41. Egelston, C. A. *et al.* Resident memory CD8+ T cells within cancer islands mediate survival in breast cancer patients. *JCI Insight* (2019).

doi:10.1172/jci.insight.130000

42. Braumuller, H. *et al.* T-helper-1-cell cytokines drive cancer into senescence. *Nature* **494**, 361–365 (2013).

43. Subramanian, A. *et al.* Gene set enrichment analysis: A knowledge-based approach for interpreting genome-wide expression profiles. *Proc. Natl. Acad. Sci. U. S. A.* (2005). doi:10.1073/pnas.0506580102

44. Scott, A. C. *et al.* TOX is a critical regulator of tumour-specific T cell differentiation. *Nature* (2019). doi:10.1038/s41586-019-1324-y

45. Costa-Silva, B. *et al.* Pancreatic cancer exosomes initiate pre-metastatic niche formation in the liver. *Nat Cell Biol* **17**, 816–826 (2015).

46. Wculek, S. K. & Malanchi, I. Neutrophils support lung colonization of metastasis-initiating breast cancer cells. *Nature* **528**, 413–417 (2015).

47. Duhen, T. *et al.* Co-expression of CD39 and CD103 identifies tumor-reactive CD8 T cells in human solid tumors. *Nat. Commun.* (2018). doi:10.1038/s41467-018-05072-0

48. Wagner, J. *et al.* A Single-Cell Atlas of the Tumor and Immune Ecosystem of Human Breast Cancer. *Cell* (2019). doi:10.1016/j.cell.2019.03.005

49. Canale, F. P. *et al.* CD39 expression defines cell exhaustion in tumor-infiltrating CD8+ T cells. *Cancer Res.* (2018). doi:10.1158/0008-5472.CAN-16-2684

50. Blank, C. U. *et al.* Defining ‘T cell exhaustion’. *Nat. Rev. Immunol.* (2019). doi:10.1038/s41577-019-0221-9

51. McLane, L. M., Abdel-Hakeem, M. S. & Wherry, E. J. CD8 T Cell

Exhaustion During Chronic Viral Infection and Cancer. *Annu. Rev. Immunol.* (2019). doi:10.1146/annurev-immunol-041015-055318

52. Egelston, C. A. *et al.* Human breast tumor-infiltrating CD8+ T cells retain polyfunctionality despite PD-1 expression. *Nat. Commun.* (2018). doi:10.1038/s41467-018-06653-9

53. Spitzer, M. H. *et al.* Systemic Immunity Is Required for Effective Cancer Immunotherapy. *Cell* (2017). doi:10.1016/j.cell.2016.12.022

54. Menares, E. *et al.* Tissue-resident memory CD8+ T cells amplify anti-tumor immunity by triggering antigen spreading through dendritic cells. *Nat. Commun.* (2019). doi:10.1038/s41467-019-12319-x

55. Goddard, E. T., Bozic, I., Riddell, S. R. & Ghajar, C. M. Dormant tumour cells, their niches and the influence of immunity. *Nature Cell Biology* (2018). doi:10.1038/s41556-018-0214-0

56. Aguirre-Ghiso, J. A. Models, mechanisms and clinical evidence for cancer dormancy. *Nature Reviews Cancer* (2007). doi:10.1038/nrc2256

57. Koebel, C. M. *et al.* Adaptive immunity maintains occult cancer in an equilibrium state. *Nature* **450**, 903–907 (2007).

58. Kim, S. Y. *et al.* Role of the IL-6-JAK1-STAT3-Oct-4 pathway in the conversion of non-stem cancer cells into cancer stem-like cells. *Cell. Signal.* (2013). doi:10.1016/j.cellsig.2013.01.007

59. Baccelli, I. *et al.* Identification of a population of blood circulating tumor cells from breast cancer patients that initiates metastasis in a xenograft assay. *Nat. Biotechnol.* (2013). doi:10.1038/nbt.2576

60. Slütter, B. *et al.* Dynamics of influenza-induced lung-resident memory T

cells underlie waning heterosubtypic immunity. *Sci. Immunol.* (2017). doi:10.1126/sciimmunol.aag2031

61. Welten, S. P. M., Sandu, I., Baumann, N. S. & Oxenius, A. Memory CD8 T cell inflation vs tissue-resident memory T cells: Same patrollers, same controllers? *Immunological Reviews* (2018). doi:10.1111/imr.12649

62. Pereira, B. I. *et al.* Senescent cells evade immune clearance via HLA-E-mediated NK and CD8+ T cell inhibition. *Nat. Commun.* (2019). doi:10.1038/s41467-019-10335-5

63. Cox, T. R. *et al.* LOX-mediated collagen crosslinking is responsible for fibrosis-enhanced metastasis. *Cancer Res.* (2013). doi:10.1158/0008-5472.CAN-12-2233

64. Goddard, E. T. *et al.* The rodent liver undergoes weaning-induced involution and supports breast cancer metastasis. *Cancer Discov.* (2017). doi:10.1158/2159-8290.CD-16-0822

65. Quail, D. F. *et al.* Obesity alters the lung myeloid cell landscape to enhance breast cancer metastasis through IL5 and GM-CSF. *Nat. Cell Biol.* (2017). doi:10.1038/ncb3578

66. Rachman-Tzemah, C. *et al.* Blocking Surgically Induced Lysyl Oxidase Activity Reduces the Risk of Lung Metastases. *Cell Rep.* (2017). doi:10.1016/j.celrep.2017.04.005

67. O'Reilly, M. S. *et al.* Angiostatin: A novel angiogenesis inhibitor that mediates the suppression of metastases by a lewis lung carcinoma. *Cell* (1994). doi:10.1016/0092-8674(94)90200-3

68. Obradović, M. M. S. *et al.* Glucocorticoids promote breast cancer metastasis. *Nature* (2019). doi:10.1038/s41586-019-1019-4

69. Albrengues, J. *et al.* Neutrophil extracellular traps produced during inflammation awaken dormant cancer cells in mice. *Science (80-.).* (2018). doi:10.1126/science.aao4227

70. Brummelman, J. *et al.* Development, application and computational analysis of high-dimensional fluorescent antibody panels for single-cell flow cytometry. *Nat. Protoc.* (2019). doi:10.1038/s41596-019-0166-2

71. Picelli, S. *et al.* Full-length RNA-seq from single cells using Smart-seq2. *Nat. Protoc.* (2014). doi:10.1038/nprot.2014.006

72. Reimand, J. *et al.* Pathway enrichment analysis and visualization of omics data using g:Profiler, GSEA, Cytoscape and EnrichmentMap. *Nat. Protoc.* (2019). doi:10.1038/s41596-018-0103-9

73. Siliņa, K., Burkhardt, C., Casanova, R., Solterman, A. & van den Broek, M. A Quantitative Pathology Approach to Analyze the Development of Human Cancer-Associated Tertiary Lymphoid Structures. in *Methods in Molecular Biology* (2018). doi:10.1007/978-1-4939-8709-2_5

74. Goldrath, A. W., Luckey, C. J., Park, R., Benoist, C. & Mathis, D. The molecular program induced in T cells undergoing homeostatic proliferation. *Proc. Natl. Acad. Sci. U. S. A.* (2004). doi:10.1073/pnas.0407417101

Figure 1

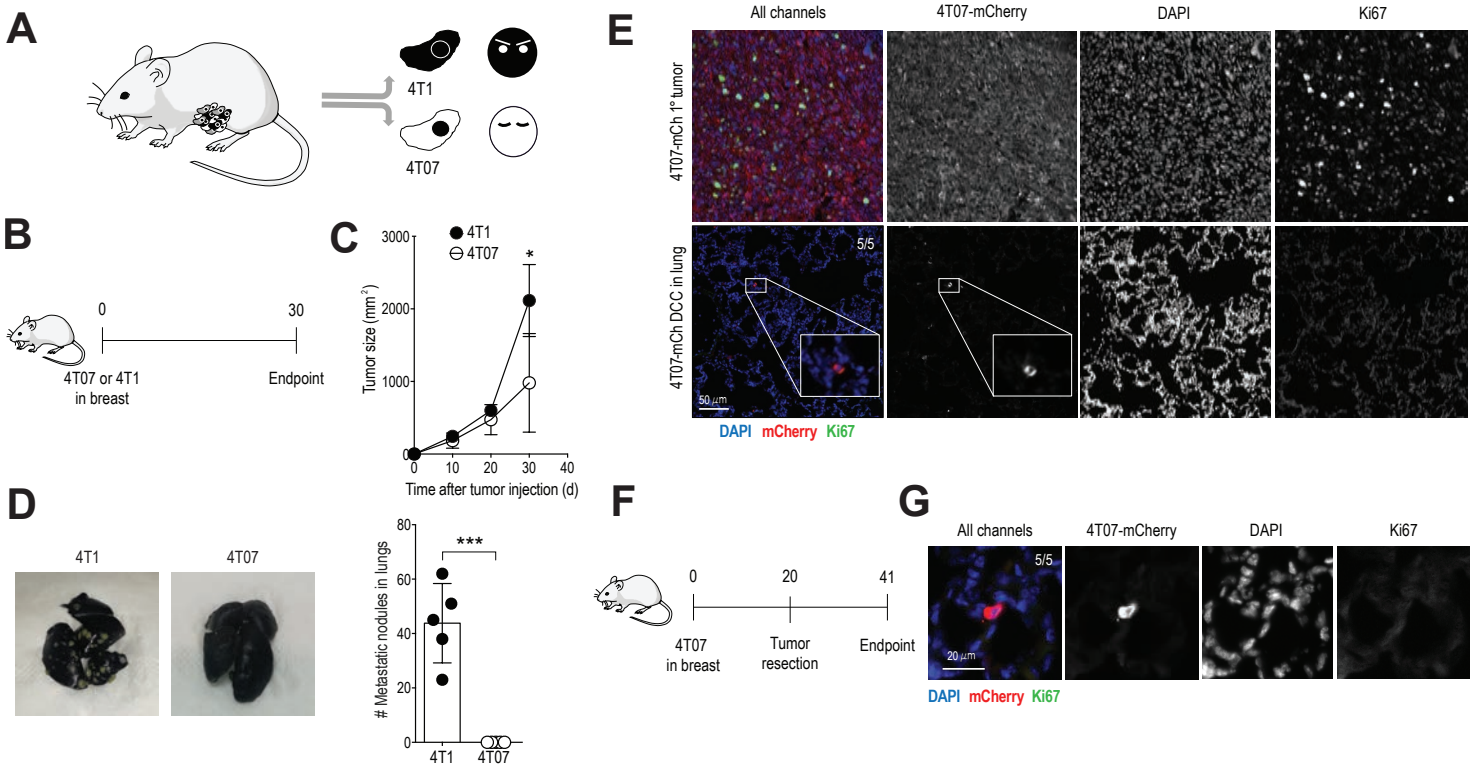
A
4T1
4T07
B
0
30
4T07 or 4T1
in breast
Endpoint
C
4T1
4T07
Tumor size (mm²)
Time after tumor injection (d)
D
4T1
4T07
Metastatic nodules in lungs
***
E
All channels
4T07-mCherry
DAPI
Ki67
4T07-mCh 1° tumor
4T07-mCh DCC in lung
5/5
50 μm
DAPI mCherry Ki67
F
0
20
41
4T07
in breast
Tumor
resection
Endpoint
G
All channels
4T07-mCherry
DAPI
Ki67
5/5
20 μm
DAPI mCherry Ki67

Figure 2

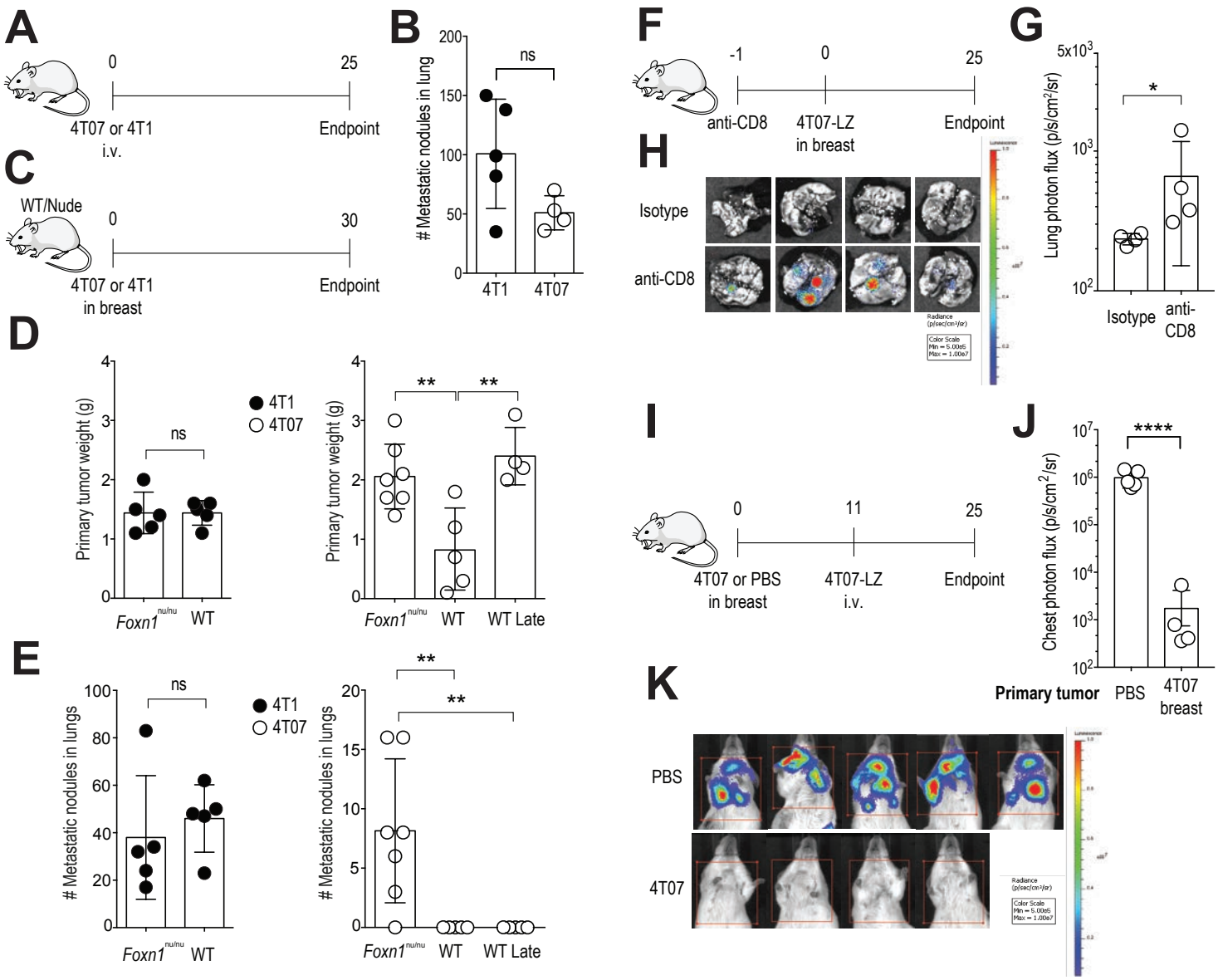
A
0
25
4T07 or 4T1
i.v.
Endpoint
B
Metastatic nodules in lung
ns
4T1
4T07
C
WT/Nude
0
30
4T07 or 4T1
in breast
Endpoint
D
Primary tumor weight (g)
ns
4T1
4T07
**
**
Foxn1nu/nu
WT
WT Late
E
Metastatic nodules in lungs
ns
4T1
4T07
**
**
Foxn1nu/nu
WT
WT Late
F
-1
0
25
anti-CD8
4T07-LZ
in breast
Endpoint
G
Lung photon flux (p/s/cm2/sr)
*
Isotype
anti-CD8
H
Isotype
anti-CD8
I
0
11
25
4T07 or PBS
in breast
4T07-LZ
i.v.
Endpoint
J
Chest photon flux (p/s/cm2/sr)
****
Primary tumor
PBS
4T07
breast
K
PBS
4T07

Figure 3

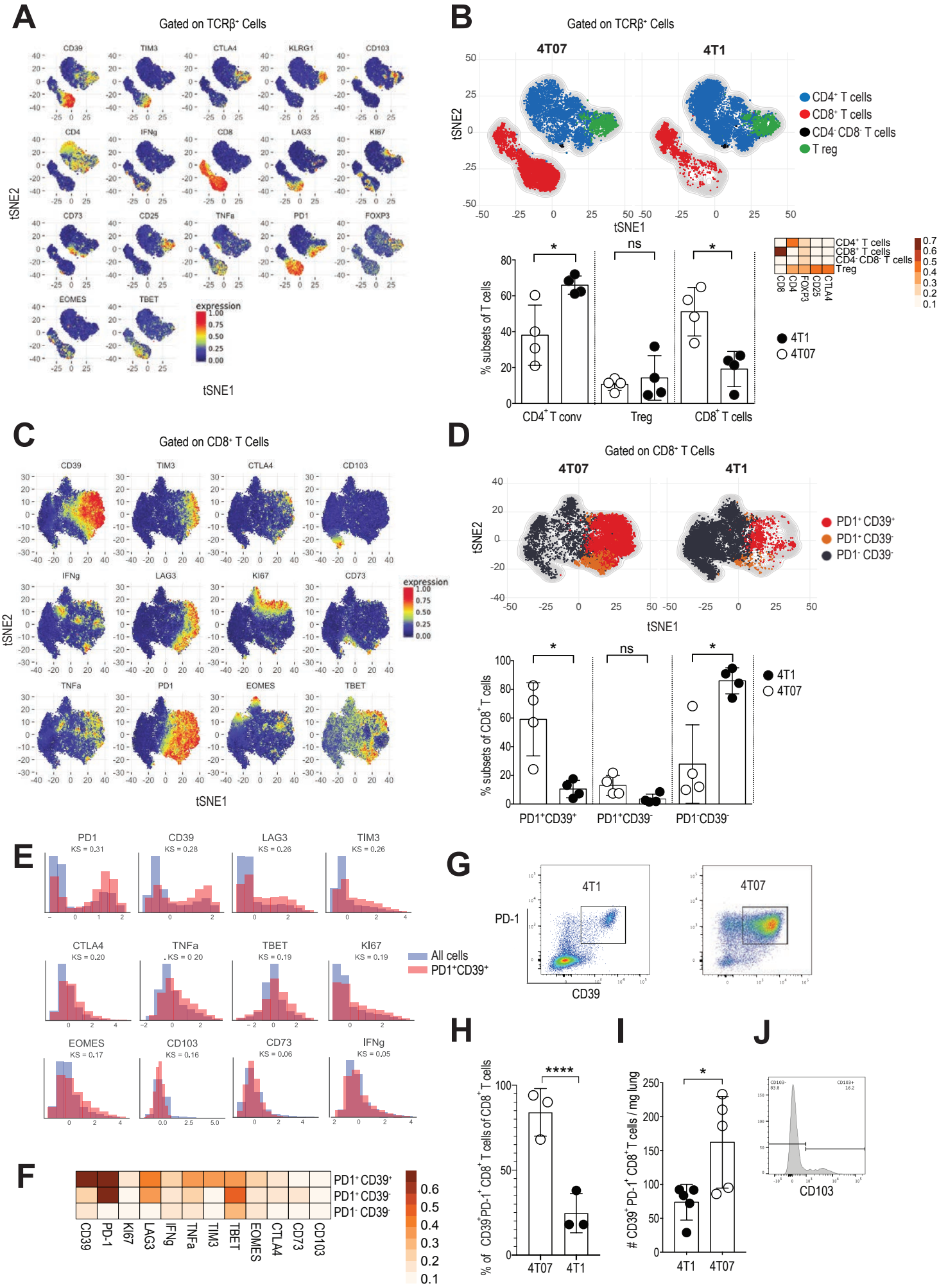
A
Gated on TCRβ+ Cells
CD39
TIM3
CTLA4
KLRG1
CD103
CD4
IFNg
CD8
LAG3
KI67
CD73
CD25
TNFa
PD1
FOXP3
EOMES
TBET
expression
tSNE2
tSNE1
B
Gated on TCRβ+ Cells
4T07
4T1
CD4+ T cells
CD8+ T cells
CD4- CD8- T cells
T reg
% subsets of T cells
CD4+ T conv
Treg
CD8+ T cells
4T1
4T07
C
Gated on CD8+ T Cells
D
Gated on CD8+ T Cells
PD1+ CD39+
PD1+ CD39-
PD1- CD39-
% subsets of CD8+ T cells
PD1+CD39+
PD1+CD39-
PD1-CD39-
E
PD1
CD39
LAG3
TIM3
CTLA4
TNFa
TBET
KI67
EOMES
CD103
CD73
IFNg
All cells
PD1+CD39+
F
G
4T1
4T07
PD-1
CD39
H
% of CD39+PD-1+ CD8+ T cells of CD8+ T cells
I
CD39+ PD-1+ CD8+ T cells / mg lung
J
CD103

Figure 4

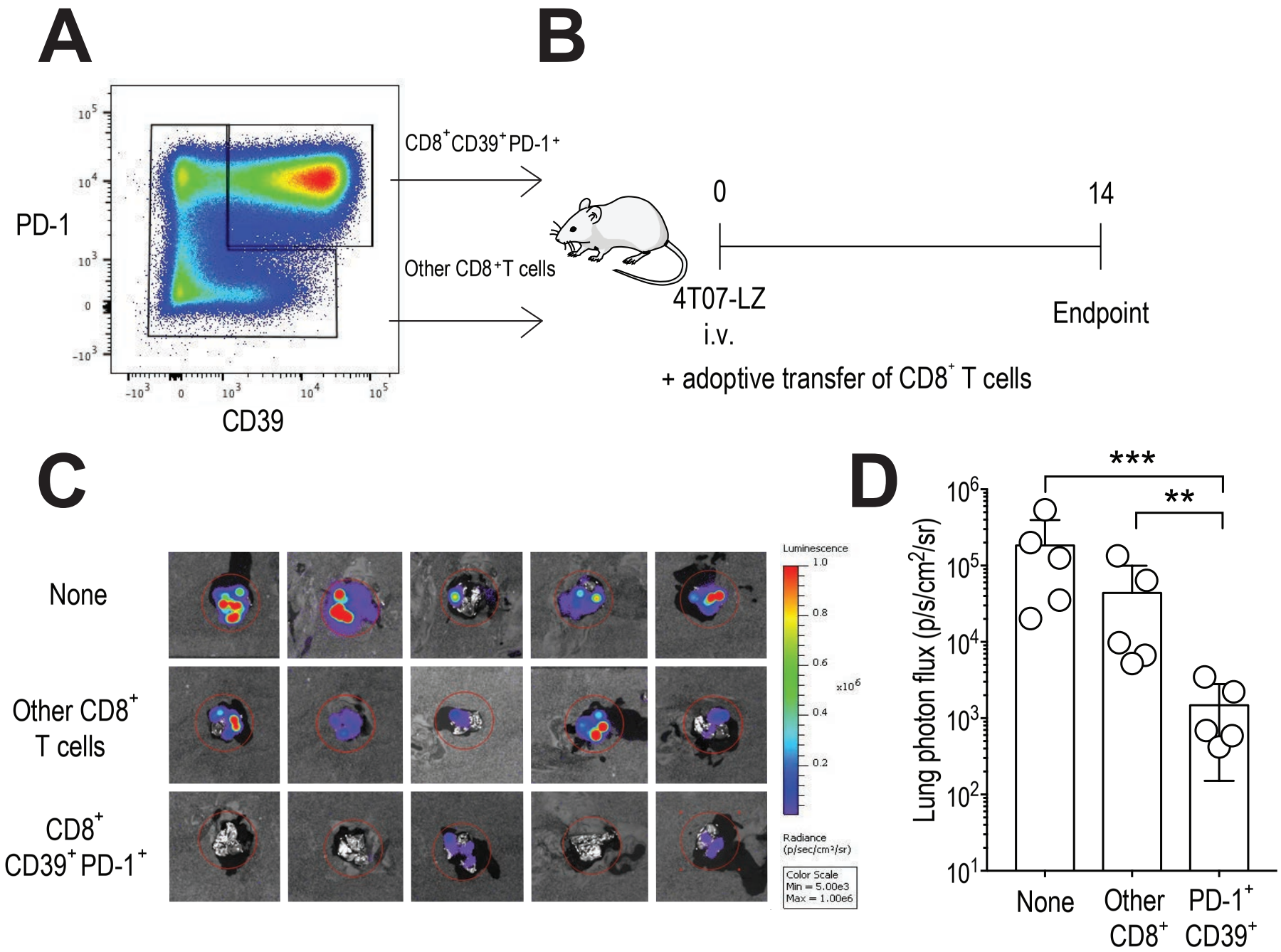
A
PD-1
CD39
CD8+CD39+PD-1+
Other CD8+T cells
B
0
14
4T07-LZ
i.v.
Endpoint
+ adoptive transfer of CD8+ T cells
C
None
Other CD8+
T cells
CD8+
CD39+PD-1+
Luminescence
Radiance
(p/sec/cm²/sr)
Color Scale
Min = 5.00e3
Max = 1.00e6
D
***
**
Lung photon flux (p/s/cm2/sr)
None
Other
CD8+
PD-1+
CD39+

Figure 5

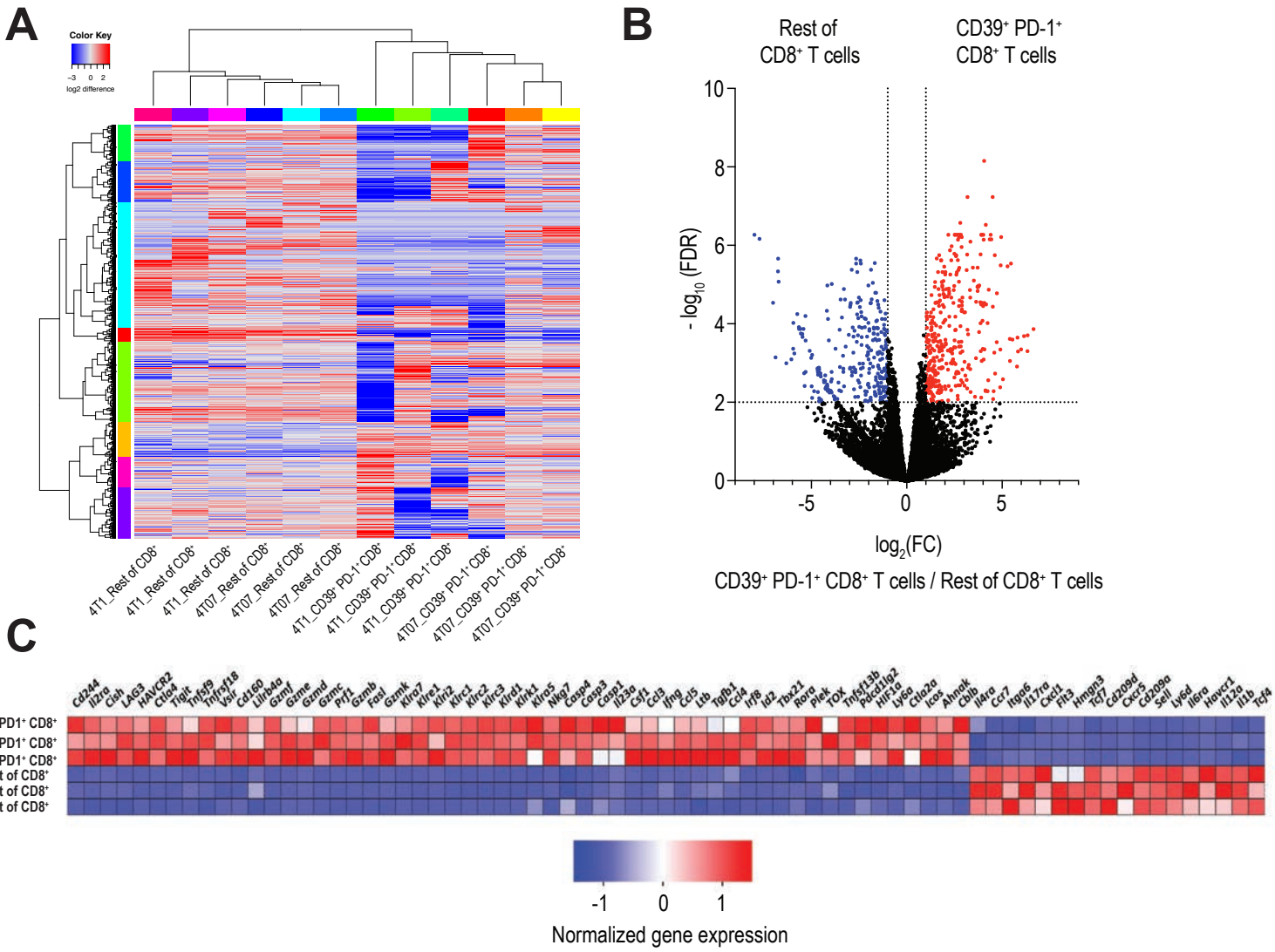
A
Color Key
log2 difference
4T1_Rest of CD8+
4T1_CD39+ PD-1+ CD8+
4T07_Rest of CD8+
4T07_CD39+ PD-1+ CD8+
B
Rest of CD8+ T cells
CD39+ PD-1+ CD8+ T cells
- log10 (FDR)
log2(FC)
CD39+ PD-1+ CD8+ T cells / Rest of CD8+ T cells
C
CD39+ PD1+ CD8+
Rest of CD8+
Normalized gene expression

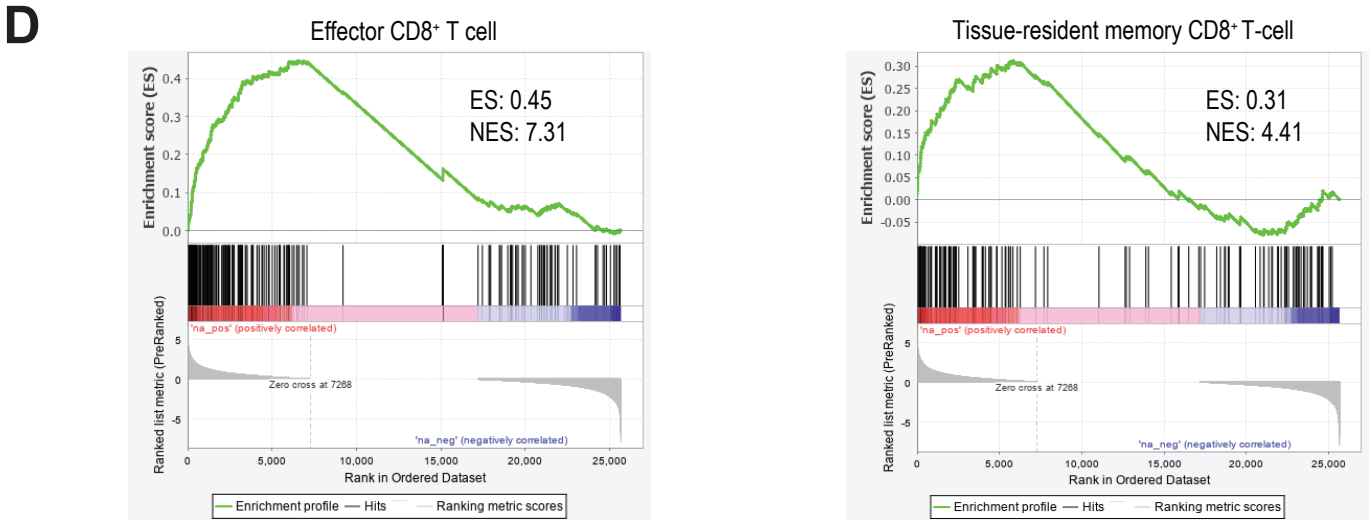
D
Effector CD8+ T cell
ES: 0.45
NES: 7.31
Tissue-resident memory CD8+ T-cell
ES: 0.31
NES: 4.41
Enrichment score (ES)
Ranked list metric (PreRanked)
Rank in Ordered Dataset
Zero cross at 7268
Enrichment profile
Hits
Ranking metric scores

Figure 6

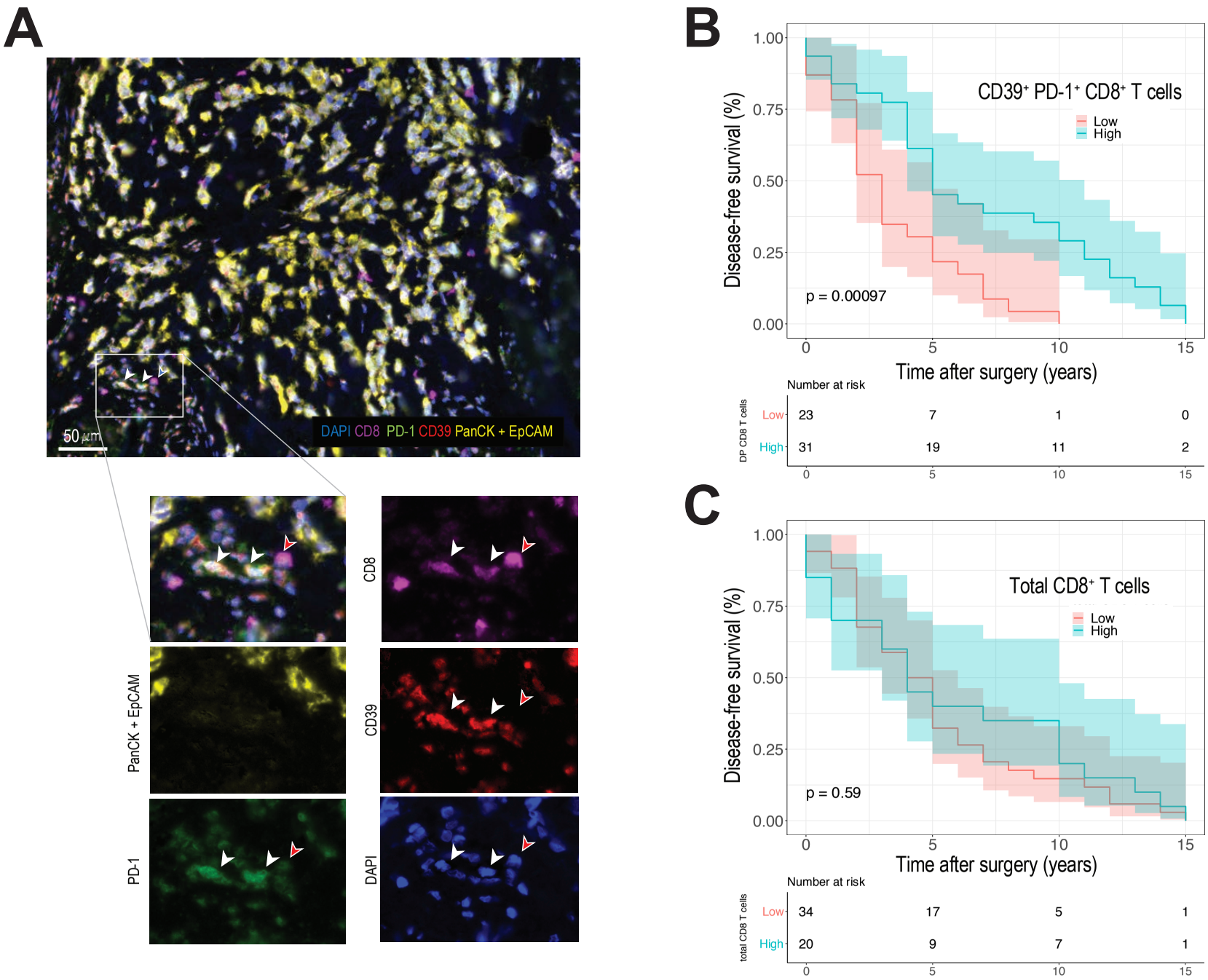
A
50 µm
DAPI CD8 PD-1 CD39 PanCK + EpCAM
PanCK + EpCAM
PD-1
CD8
CD39
DAPI
B
CD39⁺ PD-1⁺ CD8⁺ T cells
Low
High
p = 0.00097
Disease-free survival (%)
Time after surgery (years)
Number at risk
DP CD8 T cells
Low 23 7 1 0
High 31 19 11 2
C
Total CD8⁺ T cells
Low
High
p = 0.59
Disease-free survival (%)
Time after surgery (years)
Number at risk
total CD8 T cells
Low 34 17 5 1
High 20 9 7 1

Clinicopathological parameters n=54			
	N°	%	Univariate-Cox *p* value
Age at initial diagnosis			0.14
Age < 55	27	50	
Age ≥ 55	27	50	
Tumor (T) stage			0.0049
T1	18	33.5	
T2	29	53.5	
T3	4	7	
T4	3	6	
Nodal (N) stage			0.64
Negative	23	42.5	
Positive	31	57.5	
Tumor grade			0.074
Grade 1	3	5.5	
Grade 2	21	39	
Grade 3	30	55.5	
ER status			0.00077
Negative	9	16.5	
Positive	45	83.5	
PR status			0.53
Negative	15	28	
Positive	39	72	
Her2 status			0.82
Negative	37	66.5	
Positive	17	31.5	
Molecular subtype			0.0013
Luminal A	20	37	
Luminal B	25	46	
Her2	1	2	
TN	8	15	